Catastrophe-Concept-Based Cumulus Parameterization: Correction of Systematic Errors in the Precipitation Diurnal Cycle over Land in a GCM

WINSTON C. CHAO

Global Modeling and Assimilation Office, NASA Goddard Space Flight Center, Greenbelt, Maryland

(Manuscript received 23 January 2013, in final form 8 July 2013)

ABSTRACT

The onset of cumulus convection in a grid column is a catastrophe, also known as a subcritical instability. Accordingly, in designing a cumulus parameterization scheme the onset of cumulus convection requires that a parameter crosses a critical value and the termination of cumulus convection requires that the same or a different parameter crosses a different critical value. Once begun, cumulus convection continues to exist, regardless of whether the onset criterion is still met, until the termination criterion is met. Also, the intensity of cumulus precipitation is related to how far the state is from the termination, not the onset, criterion.

The cumulus parameterization schemes currently in use in GCMs, however, treat the onset of cumulus convection as a supercritical instability; namely, convection is turned on when a parameter exceeds a critical value and is turned off when the same parameter falls below the same critical value. Also, the intensity of cumulus precipitation is related to how far this critical value has been exceeded. Among the adverse consequences of the supercritical-instability-concept-based cumulus parameterization schemes are that over relatively flat land the precipitation peak occurs around noon—4–6 h too soon—and that the amplitude of the precipitation diurnal cycle is too weak.

Based on the above-mentioned concept, a new cumulus parameterization scheme was designed by taking advantage of the existing infrastructure of the relaxed Arakawa–Schubert scheme (RAS), but replacing RAS's guiding principle with the catastrophe concept. Test results using NASA's Goddard Earth Observing System GCM, version 5 (GEOS-5), show dramatic improvement in the phase and amplitude of the precipitation diurnal cycle over relatively flat land.

1. Introduction

The simulation of the precipitation diurnal cycle (PDC) over land using traditional general circulation models[1] (GCMs) has been a long-standing challenge. Over most of the land, in less mountainous regions of the globe, the simulated PDC in traditional GCMs exhibits a peak around noon, 4–6 h ahead of the observed cycle (Randall et al. 1991; Dai et al. 1999; Bechtold et al. 2004; Lee et al. 2007b; among many others). Also, the amplitude of the simulated PDC is too weak.[2] Increasing horizontal resolution does not ameliorate this problem, as long as the existing cumulus parameterization schemes are employed and individual clouds are not resolved (Dirmeyer et al. 2012). The poorly simulated PDC has adverse effects on the surface energy budget, the atmospheric branch of the hydrological cycle, and the cloud–radiation interactions. These defects have a negative impact on GCMs' performance in weather and climate forecasts and in data assimilation.

Recently, the practice of replacing the parameterizations of moist and boundary layer processes in GCMs with a cloud-resolving model (CRM) [the so-called superparameterization (SP) or multiscale modeling framework (MMF)] has led to significant improvement in the

[1] By traditional GCMs we mean GCMs in which individual cumulus clouds are not resolved and cumulus parameterization is used. They serve as the host GCMs to multiscale modeling framework (MMF) models.

[2] An exception is over high mountains, such as the Andes and the Himalayas, but this exception is eliminated when the thermal effects of subgrid-scale topographic variation are parameterized (Chao 2012).

Corresponding author address: Dr. Winston C. Chao, Global Modeling and Assimilation Office, NASA Goddard Space Flight Center, Mail Code 610.1, 8800 Greenbelt Rd., Greenbelt, MD 20771.
E-mail: winston.c.chao@nasa.gov

DOI: 10.1175/JAS-D-13-022.1

simulation of the PDC and the Madden–Julian oscillation (MJO) [e.g., Khairoutdinov and Randall (2006); with setup developed by Grabowski et al. (2006), Tao et al. (2009), Pritchard and Somerville (2009), and Khairoutdinov et al. (2008)]. Khairoutdinov et al. (2008) have also demonstrated the superiority of SP/MMF in simulating the interannual variability—with the expectation that if SP/MMF is coupled with an oceanic GCM, it will improve the performance of the El Niño simulation. Global CRMs have also reached similar or greater performance levels (e.g., Satoh et al. 2008; Putman and Suarez 2011).

However, SP/MMF models and global CRMs will not be feasible tools for long-term climate simulations in the foreseeable future because of their exorbitant (more than 200 times more costly than the traditional GCM) computational cost. Hence, there is intense interest in the modeling community in improving the GCM physics parameterizations through a combination of theoretical work and analysis of observed and/or CRM-simulated datasets so as to substantially close the performance gap between traditional GCMs and SP/MMF/global CRM models. Thus, the long-standing crucial question is what insight one can gain from observed and/or CRM-simulated datasets that can be used to improve GCM parameterizations. In other words, what is missing or wrong in the current model physical parameterizations, particularly in the cumulus parameterization?

There have been attempts to answer this question. Recently, Rio et al. (2009) and Grandpeix and Lafore (2010) showed that incorporation of wakes (also called density currents) as a factor in the triggering function in a cumulus parameterization scheme derived from Emanuel (1991) gave impressive improvement in simulating the PDC over flat land in a single-column model. In a similar vein of allowing turbulent kinetic energy (TKE) to overcome convective inhibition (CIN; the detailed definition will be discussed later), Hohenegger and Bretherton (2011) extended a shallow convection scheme into a deep convection scheme.

While we have a generally positive view of these CIN–TKE approaches, we would like to answer the aforementioned GCM deficiency question in a different way and to apply the answer to designing a new cumulus parameterization scheme using the infrastructure of an existing cumulus parameterization scheme. The expectation is that this new cumulus parameterization scheme will be able to capture the essence of what a CRM can do and thereby improve the GCM simulation. This paper focuses on the improvement of the PDC simulation over land. Other possible improvements will be investigated in a future study.

The structure of this paper is as follows. Section 2 explains our idea, which comes from the catastrophe concept. Section 3 shows why traditional cumulus parameterization schemes fail to simulate PDC correctly. Section 4 shows how our conceptual solution is used to design a new cumulus parameterization scheme, taking advantage of the infrastructure of the relaxed Arakawa–Schubert cumulus parameterization scheme (Moorthi and Suarez 1992). In section 5 our approach of cumulus parameterization is shown to be fundamentally different from the approaches based on the Arakawa–Schubert quasi-equilibrium assumption and its relaxed forms. Section 6 gives some GCM test results of our solution. Some remarks and a summary are presented in section 7.

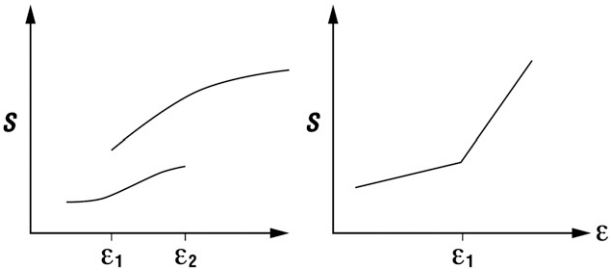

FIG. 1. (left) A schematic diagram depicting multiple equilibrium states between ε_1 and ε_2. When the state is in the lower branch and ε increases past ε_2, the state jumps to the upper branch. When in the upper branch and ε decreases past ε_2, the state stays in the upper branch. It jumps back to the lower branch only when ε decreases past ε_1. If the upper branch represents the convective regime, then the onset and termination of convection have different criteria. (right) A schematic diagram of noncatastrophe transition. There is only one criterion determining both onset and termination of a new regime.

2. The concept of catastrophe and convective initiation and termination criteria

A catastrophe is a rapid transition of a dynamical system from one (quasi) equilibrium to another. For a given set of boundary conditions, a dynamical system can have multiple stable (quasi-) equilibrium states if it is sufficiently nonlinear. When the boundary conditions or the internal characteristics of the dynamical system are changed, a stable (quasi) equilibrium can disappear and the dynamical system transits to another (quasi) equilibrium. This transit is usually quite abrupt. Figure 1 shows a schematic picture of the states of such a dynamical system. The dynamical system jumps from one type of state (the lower branch) to another type (the upper branch) when a parameter ε representing an external forcing, a boundary condition, or an internal characteristic increases and passes a critical value ε_2. However, a reduction of ε passing ε_2 does not bring the dynamical system back to the first type of state; ε has to become

lower than ε_1 for the dynamical system to jump back to the first type of state. For more complicated dynamical systems, ε may be a function of many parameters. Catastrophe is also known as structural instability, subcritical instability, finite-amplitude instability, explosive instability, and the jump in a hysteresis loop. In laymen's terms a catastrophe is the rapid change of a system when it reaches a "tipping point" (e.g., $\varepsilon = \varepsilon_2$). An important part of studying a catastrophe is to explain why the tipping point exists. Section 2 of Chao (1985) gives an elementary introduction to catastrophes. Many examples of atmospheric catastrophes are given in Chao (2008).

The initiation of cumulus convection—the rapid transition from a nonconvective state to a convective state—is an atmospheric catastrophe. For the initiation to occur, a certain criterion or set of criteria (often confusingly called the convective triggering function[3]) has to be satisfied. Once the initiation has started, whether the same criterion, or set of criteria, is still satisfied is irrelevant; the system stays in the convective regime. This concept holds not only for individual penetrative cumulus clouds but also for cumulus convection in a model grid column, since the latter is no more than a collection of individual cumulus clouds. Thus, in our design of cumulus parameterization, the convective initiation criterion that we impose becomes irrelevant once cumulus convection starts. It then takes a different convective termination criterion to stop the convection. This is a core concept of this paper, which distinguishes our work from all previous designs of cumulus parameterization scheme used in GCMs and mesoscale models with the exception of the wake (CIN–TKE) approach (to be discussed), which is implicitly consistent with our approach.

In previous designs, only one critical value ε_1 is used to determine both the initiation and the termination of convection. When ε (which may be a function of many variables) exceeds ε_1, convection is allowed and when it drops below ε_1, convection is disallowed (Fig. 1b). Also, the intensity of convection is a function of how much ε_1 has been exceeded, that is, $\varepsilon - \varepsilon_1$. Thus, in our new design modeled on the catastrophe concept, the intensity of convection is not related to how much the initiation criterion is exceeded, but to how far away the state is from the termination criterion. This is the second core concept of our approach.

The support for our idea comes from a simulation of cumulus convection over the Atmospheric Radiation Measurement Program (ARM) U.S. Southern Great Plains site for 27 June 1997 with a 2D CRM [see Figs. 4a and 4c of Guichard et al. (2004, hereafter G04), which are reproduced as Fig. 2] with a 512-km domain and a 2-km horizontal grid size. That particular day was chosen because of the absence of synoptic systems. Thus, the variation in convection that day was solely due to the diurnal variation of surface fluxes and, to a much lesser extent, radiation. This allowed the diurnal variation in convection to be studied in isolation.

Figure 2 shows the domain-averaged quantities. In the hours prior to 1030 local solar time (LST), CIN[4] [the negative buoyancy below the level of free convection (LFC)] prevented cumulus convection from rising until CIN became almost zero, but once the cumulus convection started, the rise of CIN posed no inhibition at all to cumulus convection, which continued until the convective available potential energy (CAPE) was almost exhausted, when CIN was near its peak. CAPE is defined as the vertical integral of buoyancy from the level of free convection up to the level of zero buoyancy for a cloud with no entrainment, whereas CIN is the integral of the negative buoyancy from the planetary boundary layer top to the level of free convection. Both CAPE and CIN have positive values. In essence, this figure shows a convective initiation criterion of CIN decreasing passing a critical value ($\mathrm{CIN}_c \sim 1\,\mathrm{J\,kg^{-1}}$) and a separate convective termination criterion of CAPE decreasing past a critical value ($\mathrm{CAPE}_c \sim 100\,\mathrm{J\,kg^{-1}}$, or becoming negligible compared with its peak value). Figure 3 shows a schematic depiction of the on and off states of cumulus convection as a function of CAPE and CIN. Note that CAPE and CIN are highly negatively correlated. An important feature in Fig. 2 is that the valve that opens for cumulus convection in a grid column takes time to be completely open, as indicated by the weak drop of CAPE between 1030 and 1430 LST in Fig. 2. Cumulus convection in a grid column first starts with small thermals breaking through the CIN barrier and is then

[3] In the literature on cumulus parameterization, the term *triggering function* is often used to mean a criterion that has to be satisfied for cumulus convection not just to start but to continue to exist; that usage is inconsistent with the real meaning of the word *trigger*, which is involved only in the starting of an event but not in the continuation of the event. Strictly speaking, triggering function is a misnomer, since no trigger is introduced to the modeled air column. By a trigger we mean an amount of energy that is introduced smoothly or abruptly to a dynamical system to allow the latter to overcome an energy barrier in order for it to jump from one (quasi-) equilibrium state to another. We prefer the term *initiation criterion* to the term *triggering function*.

[4] CIN, as used in this work, is computed the same way as cloud work function for a zero-entrainment-rate cloud type is computed, except that the integration goes from the top of boundary layer to LFC. In the code this is done by 1) copying the code that computes the cloud work function, 2) specifying the entrainment rate as zero, and 3) stopping the computation at LFC.

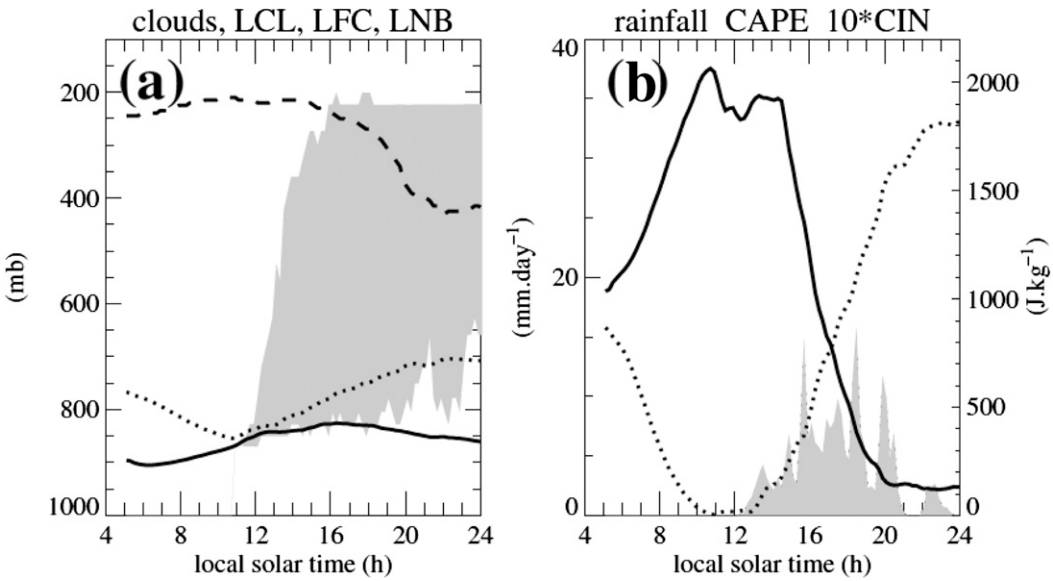

FIG. 2. A reproduction of (a) Fig. 4a and (b) Fig. 4c in G04. In (a) the solid curve depicts the LCL, the dotted curve depicts the LFC, and the dashed curve depicts the level of no buoyancy (LNB); the shaded region depicts the vertical domain occupied by clouds. In (b) the solid curve depicts CAPE and the dotted curve depicts CIN multiplied by 10; the shading depicts precipitation. In (a) the convection takes more than 4 h to reach its peak height. In (b) CIN prohibits convection until it becomes very small; however, once convection starts, the increasing CIN presents no obstacle for convection to continue. It also shows the dramatic buildup of CAPE prior to the onset of convection.

followed by some of them growing larger and reaching greater heights. This process takes more than 4 h to complete according to Fig. 2a. Only after 1430 LST does the valve become completely open and CAPE starts to drop dramatically.

The explanation for the inability of CIN (until it gets near its peak and when CAPE is essentially exhausted) to suppress convection once it commences is that the thermals in the boundary layer grow larger as a result of density currents generated by the cloud-scale downdraft (Kuang and Bretherton 2006; Khairoutdinov and Randall 2006) and these larger thermals have enough energy to overcome the local CIN. At the first start of convection, clouds can only reach limited heights. Later, some of them can grow taller with the help of convective organization because of cloud clustering (Mapes and Neale 2011). In this growth CIN, a grid-domain-mean quantity, presents no obstacle. Moreover, once convection starts, CIN is no longer uniform throughout the grid domain and the vertical motion associated with the large thermals can reduce local CIN. This spatial variation of CIN within a GCM gridbox domain was found in previous CRM simulations (e.g., Chaboureau et al. 2004).

Our concept of different convective initiation and termination criteria can be easily infused into any cumulus parameterization scheme. Our cumulus parameterization is named catastrophe-concept-based cumulus parameterization (C-CUP). In the next section we will discuss why the noncatastrophe characteristics of the currently used cumulus parameterization schemes are responsible for the incorrect phase and amplitude in simulated PDC.

3. The reason why noncatastrophe cumulus parameterization schemes yield the wrong phase and a weak amplitude in the PDC

A noncatastrophe-concept-based cumulus parameterization scheme adjusts the state of the grid column back toward a critical state and the amount of adjustment is proportional to how far the critical state has been exceeded. The state of the grid column is normally described by a quantity Q that is a measure of the convective instability and the critical state Q_c is often

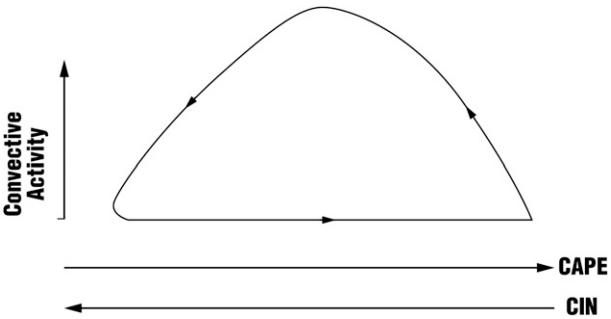

FIG. 3. A schematic depiction of the on and off states of cumulus convection as a function of CAPE and CIN.

a time-mean value of the observed Q. When Q is greater than Q_c, convection is allowed and the precipitation rate P is proportional to how much Q has exceeded Q_c at the time when the cumulus parameterization scheme is called in the model. If Q falls below Q_c, there is no cumulus convection. In other words the noncatastrophe cumulus parameterization schemes adjust Q to/toward Q_c. Since Q_c is a constant, in cases where Q is adjusted to Q_c, as is done, for example, in the Arakawa and Schubert (1974, hereafter AS) scheme, P is proportional to how fast Q is increased by processes (both dynamical and physical) other than cumulus convection since the last time the model invoked the cumulus convection scheme. Over less mountainous regions and when there are no synoptic events, Q is mostly increased by the surface heat flux and to a much lesser degree by the radiative cooling, which does not have as large a diurnal change as the surface heat flux. Thus, with a noncatastrophe cumulus parameterization scheme, in cases of typical strong summer diurnal cycle cases, the peak of precipitation at these locations occurs at the time of the peak surface sensible heat flux, which is around noon—in contrast to the observed peak in late afternoon (1600–1800 LST). Also, as we will explain in the next paragraph, the precipitation peak in these instances is far less sharp than what is observed, resulting in a very weak amplitude for the PDC.

In cases where Q is only partially adjusted back to Q_c in each call of the cumulus parameterization scheme, as is done in the relaxed Arakawa–Schubert scheme (RAS) (Moorthi and Suarez 1992) with a reasonable relaxation time scale, such a tie between surface heat flux and precipitation is not completely broken; the precipitation peak can be delayed slightly from noon but certainly not by 4–6 h. Of course, if the relaxation time scale is set unrealistically large (greater than 10 h), a 4–6-h delay can be achieved, but the amplitude of the PDC becomes even more unrealistically small, and the precipitation duration is much longer than the observed 6–8 h—as illustrated in Fig. 4. Figure 4 shows a schematic diagram of the time variation of cloud work function $\mathbf{A}$ (equivalent to Q) when RAS is used, assuming a (positive half cycle) sinusoidal forcing, which mimics the forcing due to surface fluxes, in the first 12 h, beginning at 0600 LST, and followed by zero forcing in the next 12 h as denoted by the envelope of the lower branch of the diagram. During each physics time step (Δt = 30 min), $\mathbf{A}$ is increased by the forcing, which is illustrated by the slanted dotted lines. This is followed by a drop in $\mathbf{A}$ by the amount $\mathbf{A}/n$, which represents the effect of cumulus convection and is illustrated by the vertical solid lines. In other words, the intensity of the cumulus convection follows the formula of

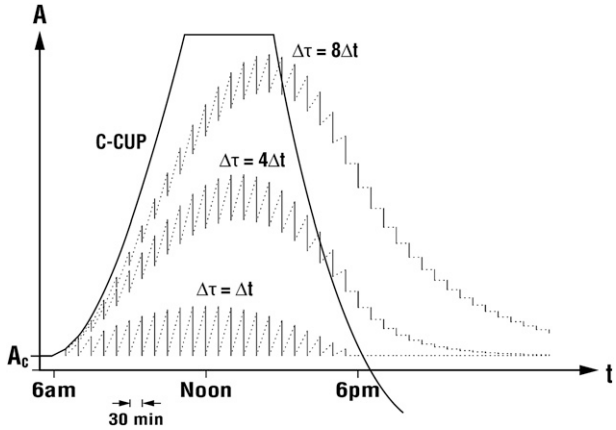

FIG. 4. For a positive-only half-sine-curve convective forcing between 0600 and 1800 LT, the time variation of $\mathbf{A}$ when the AS scheme (bottom curve) and the relaxed AS scheme (middle and upper curves) are used. The solid curve represents the time variation of $\mathbf{A}$ according to the catastrophe concept. See text for details.

$(\mathbf{A} - \mathbf{A}_c)/(n\Delta t)$ with $\mathbf{A}_c = 0$. The definition of $\mathbf{A}_c$ will be discussed in the next section. The lengths of the vertical solid lines are proportional to the precipitation rate. The lower, middle, and upper branches have n = 1, 4, and 8, respectively. The lower branch represents the AS scheme. As n increases (i.e., as the relaxation time scale increases), the peak of precipitation is increasingly more delayed from noon. With n = 8 the delay is about 2.5 h. Also, as n increases the maximum precipitation decreases and the precipitation duration increases, resulting in a much weaker PDC. These conclusions are not affected by a positive $\mathbf{A}_c$ or by an additional forcing representing the effect of radiative cooling. The solid curve in Fig. 4 shows that time variation of $\mathbf{A}$ according to the catastrophe concept. It shows that dramatic rapid buildup prior to the onset of convection when the suppression effect of CIN is recognized. Thereafter, $\mathbf{A}$ does not change much until its precipitous drop after 1430 LT, as in the CAPE curve in Fig. 2b. This rapid drop of $\mathbf{A}$ accounts for the observed maximum precipitation in the late afternoon and the short duration of precipitation.

The recent schemes based on the density current and CIN–TKE ideas, such as those of Rio et al. (2009), Grandpeix and Lafore (2010), and Hohenegger and Bretherton (2011), have assumed implicitly the catastrophe concept and are thus able to overcome the problems in the PDC simulation. However, these schemes have thus far only been tested in single-column models.

4. Design of a C-CUP scheme

Before starting, we will give a brief summary of the RAS scheme (Moorthi and Suarez 1992), which is our starting point. In RAS, a vector $\mathbf{m}$ with each element

representing the cloud-base mass flux of a cloud type is computed from

$$\mathbf{Km} = -(\mathbf{A} - \mathbf{A}_c)/\Delta\tau, \quad (1)$$

where $\mathbf{K}$ is a matrix, $\mathbf{A}$ is the cloud work function vector, $\mathbf{A}_c$ is the critical $\mathbf{A}$, and $\Delta\tau$ is the relaxation time scale. A cloud type represents clouds that reach a model level. Each element of $\mathbf{A}$ represents the cloud work function of a cloud type. In Eq. (1) $\mathbf{Km}$ represents the reduction of $\mathbf{A}$ due to cumulus convection, and the right-hand side of Eq. (1) represents the rate of depletion of $\mathbf{A}$. With some simplifications $\mathbf{K}$ is reduced to a diagonal matrix. After $\mathbf{m}$ is computed, it is used to modify the temperature and moisture profiles of a grid column according to a simplified cloud ensemble model. In the equation $\mathbf{A}_c$ is set at the observed climatologically averaged $\mathbf{A}$, $\mathbf{A}_{cc}$, from observations at the Marshall Islands (Lord et al. 1982); $\mathbf{A}$ has to be greater than $\mathbf{A}_c$ for a cloud type to exist. This is an example of the so-called triggering function. Thus, $\mathbf{A}_c$ serves as both the critical value for the convection onset criterion (i.e., $\mathbf{A} > \mathbf{A}_c$) and for the convection termination criterion (i.e., $\mathbf{A} < \mathbf{A}_c$). Also, Eq. (1) indicates that the intensity of convection is related to $\mathbf{A} - \mathbf{A}_c$, that is, how much the onset criterion has been exceeded. In the current usage in the model, prior to the modification described in this paper, $\Delta\tau$ is set at the physics time step (30 min) in a departure from the original "relaxed" idea, which sets $\Delta\tau$ greater than the physics time step.

In the remaining part of this paper, the RAS as implemented in the National Aeronautics and Space Administration (NASA) Goddard Earth Observing System GCM, version 5 (GEOS-5 GCM) (Bacmeister et al. 2006) prior to our modification is referred to as RAS and the RAS with our revisions is referred to as the catastrophe-concept-based cumulus parameterization scheme (C-CUPs) (C-CUP refers to the idea of using the catastrophe concept in cumulus parameterization and C-CUPs refers to the particular scheme that we proposed in this work). It is stressed that once RAS is infused with the catastrophe concept, it no longer follows the Arakawa–Schubert quasi-equilibrium assumption or its relaxed form as in RAS. Therefore, by infusing the catastrophe concept into RAS, we are really creating a new cumulus parameterization scheme, but we take advantage of the infrastructure of RAS, such as the computation of $\mathbf{A}$ and $\mathbf{K}$ and the computation of temperature and moisture tendencies due to cumulus parameterization—through the simplified cloud model—once $\mathbf{m}$ is obtained.

In accordance with the concept explained above, the infusion of our idea into RAS involves several steps. The first is to determine the cumulus existence status of the preceding physics (CESP) time step (CESP = true or false) for each grid column. To simplify matters, this is not done separately for each cloud type. If any cumulus cloud type exists in the preceding step, then CESP is true. Next, CIN is computed and is used to disallow cumulus convection if CIN is greater than CIN_c, provided CESP is false. Convection is turned on and is allowed for all cloud types with some restriction to be described below, if CESP is false and if CIN becomes lower than CIN_c. This is the convective initiation criterion. If CESP is true, then CIN is disregarded and convection is allowed to continue. When CESP is true, the only criterion, the convective terminating criterion, that would deny all cloud types' existence is that CAPE is less than CAPE_c, which is to be given in the next subsection. Alternatively, we could use CIN increasing and passing a critical value as the termination criterion.

For the initial step of an experiment CESP is assumed to be "false," unless it can be otherwise determined from a preceding integration. This should not be a problem for long-term climate integrations. For short-term weather forecasts, the cumulus existence status in the initial conditions should be ascertained from observations.

As pointed out above, our revision to RAS keeps the form of Eq. (1) but changes its meaning. Also, the definitions of $\mathbf{K}$, $\mathbf{m}$, and $\mathbf{A}$ are retained. However, $\mathbf{A}_c$ is replaced by $\mathbf{A}_0$, which has a different meaning and whose value is to be given. And the value of $\Delta\tau$ is changed.

a. *The choice of CIN_c*

In the experiments reported in this paper, CIN_c is set at $1\,\mathrm{J\,kg^{-1}}$, a value roughly determined from Fig. 4d of G04. Given that our definition of CIN is not exactly the same as in G04, this is a guess estimate. CIN_c is used as a tuning parameter. The choice of CIN_c affects the starting time of convection in the PDC. Note that CIN_c is not a function of cloud type.

b. *The choices of CAPE_c and $\mathbf{A}_c$*

When the CAPE calculated at the beginning of the cumulus parameterization scheme is less than $200\,\mathrm{J\,kg^{-1}}$ (CAPE_c), convection for all cloud types is terminated by setting the cloud mass flux at the cloud base to zero for all cloud types. In accordance with the discussion above, CAPE_c should be used to replace $\mathbf{A}_c$ in Eq. (1), at least for low entraining cloud types. However, if $\mathbf{A}_c$ is set at CAPE_c, then as $\mathbf{A}$ diminishes and approaches $\mathbf{A}_c$ the rate of decrease of $\mathbf{A}$ will diminishes as well. Therefore, to ensure that convection quickly terminates as $\mathbf{A}$ gets near $\mathbf{A}_c$, we set $\mathbf{A}_c$ to be CAPE_c minus an offset, which also has a value of $200\,\mathrm{J\,kg^{-1}}$. In other words, we simply set $\mathbf{A}_c$ to zero. This is done for all cloud types, for simplicity. A more refined design would have $\mathbf{A}_c$ as a function of cloud type, but we will leave this as future work.

c. The choice of relaxation time scale $\Delta\tau$

In RAS, $\Delta\tau$ has been given different values, varying from 30 min (the GEOS-5 GCM physics time step) to several hours in separate experiments to assess the optimal value. Because of the modifications associated with CIN and $\mathbf{A}_c$ as described in the preceding subsections, $\mathbf{A}$ is quite large compared with $\mathbf{A}_c$ when the cumulus convection first starts in a PDC. Thus, setting $\Delta\tau$ to 30 min, the physics time step interval, which would imply trying to reduce $\mathbf{A}$ to $\mathbf{A}_c$ in 30 min, would obviously not be correct; $\Delta\tau$ should be set at a much larger value. Figure 2b shows a steep drop of CAPE in 6 h. However, it should be noted that during these 6 h, the change of CAPE is not due to convection alone, since CAPE is also increased by large-scale forcing during this period. Thus, in our experiments we set $\Delta\tau$ to be less than 6 h, namely, 3 h; $\Delta\tau$ could be a function of cloud type and this function can only be guessed at this time. Presumably, taller cloud types involve a large circulation field and they take a longer time to evolve; thus, $\Delta\tau$ should be an increasing function of cloud-top height. However, because of the lack of theoretical guidance, we will not include this variation. Also, $\Delta\tau$ should be allowed to change during the life cycle of a convective event. But, again, because of the lack of theoretical guidance, this is not done at this stage.

d. Modeling the gradual growth of taller clouds

Shallow clouds begin to form before deep clouds do, because smaller thermals first have to punch through the inversion layer above the boundary layer to provide the right environment for some of them to grow into larger thermals to get through. Also, smaller thermals have larger entrainment rates and thus detrain at lower levels to form shallower clouds. This idea, discussed by a number of authors (e.g., Grabowski et al. 2006), has been recognized as important to cumulus parameterization (e.g., Rio et al. 2009; Grandpeix and Lafore 2010). CRM support of this idea is presented in Fig. 2a. It shows that cloud-top height takes about 5 h, from 1100 to 1600 LST, to reach maximum.

Taller clouds grow out of shallow clouds. A possible method to ensure that shallow cloud types arise before taller ones do is to impose an additional condition for the taller cloud types to exist. A taller cloud type is turned on only if the next lower cloud type existed in the preceding physics time step. Once this cloud type exists, this criterion will not be invoked in the following steps. This is justified because taller clouds grow out of clouds shallower than they are and because the growth takes time. This criterion allows 30 min for the next higher cloud type to appear. However, since the model may have so many levels (and thus so many cloud types), it will take more than 4 h after the first shallowest cloud type appears for the tallest cloud type to appear. Thus, the cloud types are grouped into subsets according to their cloud-top height. Consequently, every 30 min a subset with the next higher cloud tops is added to the allowed list, if any cloud type in a subset exists in the preceding time step.

The number of subsets is predetermined so that the tallest subset is allowed to arise within 5 h of the first occurrence of the lowest subset. This value of 5 h is taken from Fig. 2a (1100–1600 LST), which shows the growth of cloud-top height. In C-CUPs we tried 10 subsets, since the physics time step is 30 min. Note that in the initial test the above-mentioned 5 h is changed to 4 h and 10 subsets are changes to 8 subsets. The drawback of this method is the existence of various possibilities of grouping and this makes the task of tuning very difficult.

An alternative method for modeling the gradual development of convection is to allow all cloud types once the onset criterion is met and to multiply a fraction f to the computed cloud-base mass fluxes for all cloud types in the first 5 h. Though crude, this method is easier to tune and is used with $f = 0.01$ in the test runs reported in section 6. With f increasing from 0.01 to 0.1 in the first 5 h, the results do not vary much. Another way to mimic a part of the delay of the onset of precipitation is to keep the output from C-CUPs in storage for two physics time steps (1 h) before passing them onto the rest of the physics package in order to simulate the water storage effect of stratiform clouds (Houze 1977). This was tested and led to better simulation of the PDC phase. A simpler way is to extend the 5 h mentioned above to 6 h. This approach is used in the experiments reported in section 6.

e. Limit imposed on maximal cloud-base mass flux

Through experimentation we have found that not imposing a maximum limit on the cloud-base mass flux [$\mathbf{m}$ in Eq. (1)] results in an excessively large ITCZ precipitation rate over the ocean. Thus, we put a limit on the cloud-base mass flux. This is purely for expediency. The simulation of the ITCZ is still a subject that requires more research. However, such a limit has the side effect of lowering the amplitude of the simulated PDC. We have found that setting this limit to $50\,\mathrm{kg\,s^{-1}}$ for each cloud type is a good compromise.

f. Summary of the procedure

If 1) there is no convective precipitation in the preceding physics time step (CESP = false) and 2) the beginning part of RAS gives a $\mathrm{CIN} > \mathrm{CIN}_c$, with $\mathrm{CIN}_c = 1\,\mathrm{J\,kg^{-1}}$, then the rest of RAS for all cloud types is bypassed.

Otherwise, RAS proceeds with two changes: $\mathbf{A}_c$ is set to zero when computing the right-hand side of Eq. (1) and $\Delta\tau$ is set at 3 h. In the first 6 h of convection after $\mathbf{m}$ is

computed, **m** is multiplied by 0.01. When CAPE at the beginning of the RAS computation is less than 200 J kg^{-1}, the rest of RAS for all cloud types is bypassed. This is the convective termination criterion in C-CUPs.

The initial condition/restart files should contain information about the existence of precipitation (CESP) in each grid column in the last physics time step of the previous model time integration. If no such information is provided, then CESP is assumed to be false.

A flowchart of our procedure for each grid column is provided in the appendix.

g. Remarks

In the wake approach (Rio et al. 2009; Grandpeix and Lafore 2010) and the CIN–TKE approach (Hohenegger and Bretherton 2011), although CIN is still taken into account after convection commences, it is countered by the lifting energy of the large thermals created by density currents and it is effectively rendered useless in suppressing convection once convection starts until it becomes very large. In the wake approach, in the computation of the lifting energy of the thermals there is an adjustable parameter to ensure that high CIN can be overcome. Our approach, through the use of the termination criterion CAPE < 200 J kg^{-1}, bypasses the need to parameterize the wakes. It is noted that the wake and CIN–TKE approaches have the catastrophe concept implicitly embedded in them.

5. The contrast with the Arakawa–Schubert quasi-equilibrium assumption

It is clear by now that, according to the above-mentioned modifications, our approach is fundamentally different from the quasi-equilibrium approach, as described in AS, and the relaxed approach, as described in RAS (Moorthi and Suarez 1992). Without taking into account the suppressing effect of CIN prior to the onset of convection, RAS does not allow the dramatic buildup of **A** in the morning hours. Also, in our approach in the afternoon hours when convection does exist, **A** is not adjusted toward $\mathbf{A}_{cc}$, but to zero. This difference is the second core concept of our work.

C-CUP's difference from the AS quasi-equilibrium assumption is supported also by Fig. 2b. This figure shows that CAPE (equivalently, **A** for the nonentraining cloud type) during the convective period starting from 1200 to about 2000 LST dropped at a much faster rate than the rate of increase between 0500 and 1100 LST when no convection existed. In view of the fact that the experiment corresponding to Fig. 2b was conducted for a day devoid of synoptic systems, the increase of CAPE between 0500 and 1100 LST was predominantly because of surface heat fluxes and, to a much lesser extent, radiative cooling. Given that similar surface heat fluxes existed in the afternoon, one can estimate that a similar amount of increase in CAPE due to surface fluxes and radiation existed between 1300 and 1900 LST as between 0500 and 1100 LST. This indicates that in the afternoon hours, the rate of decrease in CAPE due to cumulus convection is at a much greater rate than the rate of increase in CAPE due to large-scale forcing—a clear indication of a drastically different picture from the AS quasi-equilibrium assumption and from what RAS allows. C-CUPs allows this drastic change in CAPE.

RAS, by following a relaxed form of the AS assumption, allows convection to start early in a case like that of Fig. 2b, since $\mathbf{A}_{cc}$, being close to the averaged **A** of that day, is much smaller than the peak **A** reached at 1030 LST. And once convection starts, the precipitation rate generated by RAS is tied to the rate of increase of **A** by large-scale processes, which is largest at noon. The relaxation time scale only delays the peak precipitation rate by an hour or so (as we have shown in Fig. 4), resulting in a phase shift of 4 h too early in the PDC. Also, the peak precipitation rate generated by RAS—being tied to the rate of increase of **A** by large-scale processes—is much smaller than that generated by C-CUPs, which is tied to the large difference between peak **A** and $\mathbf{A}_0$.

An obvious question at this point is what to make of the conflicting supporting evidences presented in published studies in favor of the AS assumption. For example, Fig. 13 of AS shows the time rate of change of **A** is much smaller than the time rate of change of **A** due to large-scale forcing. However, it used observed data at 6-h intervals. A 6-h interval is too large to resolve the PDC (Mapes 1997) because the main precipitation episode in the PDC lasts only about 6 h (Fig. 2b). To compute the time rate of change of **A** accurately, an observation interval of 30 min or 1 h is required. The reader is also referred to Mapes (1997) for a critical review of the AS quasi-equilibrium (QE) assumption.

It is noted, however, that the need to move away from the AS QE assumption was recognized early on by many [e.g., Xu et al. 1992; see also the review by Arakawa (2004)]. This need was revisited recently by Jones and Randall (2011) with the conclusion that models using cumulus parameterization schemes based on the AS QE assumption cannot successfully simulate convective processes with a time scale shorter than 30 h. Thus, how to modify the cumulus parameterization so as to achieve the timing, degree, and speed of departure from the AS assumption that are observed in CRMs has been a challenge. C-CUPs is designed to meet this challenge.

Like the quasigeostrophic models that filter out the transient aspect of geostrophic adjustment, the AS

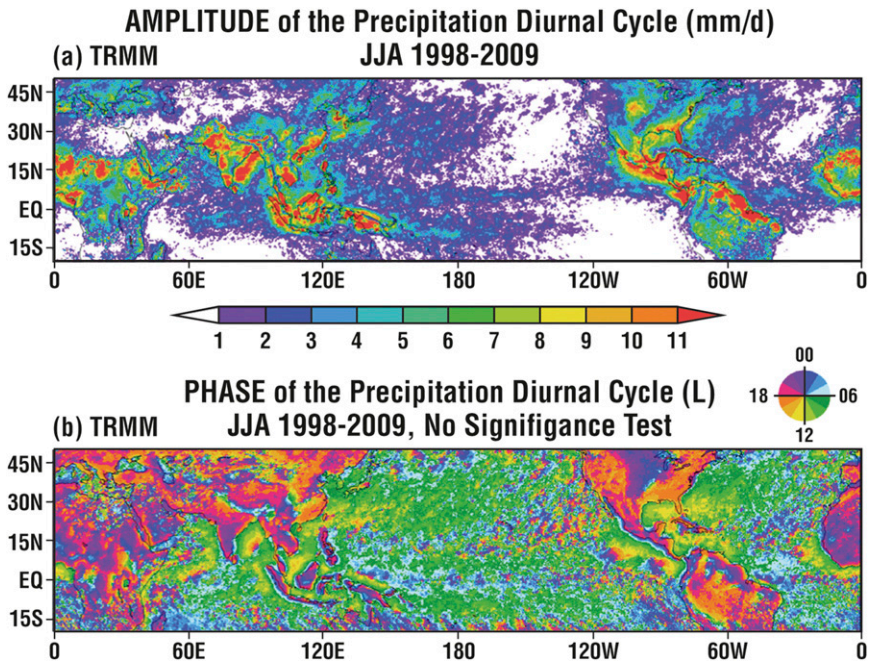

FIG. 5. Amplitude (mm day^{-1}) and phase of the JJA precipitation diurnal cycle of the TRMM data averaged over 11 years. (Courtesy of M.-I. Lee).

quasi-equilibrium assumption filters out the transient adjustment of a cloud ensemble (Schubert 2000), which includes some of the PDC and most of the ability for one cloud cluster to generate intense inertial–gravity waves to trigger another cloud cluster. A cumulus scheme based on the AS assumption can still produce PDC because of the diurnal variation in surface fluxes, which are a part of the large-scale forcing. However, the amplitude and phase of the PDC produced are incorrect, as we have explained. Likewise, the excitation of inertial–gravity waves—important for the existence of the MJO—can still be achieved by schemes based on the AS assumption and its relaxed forms but at much lower amplitudes.

RAS by adjusting $\mathbf{A}$ toward $\mathbf{A}_{cc}$ when there is convection does not guarantee that time-mean $\mathbf{A}$ is the same as $\mathbf{A}_{cc}$. However, it is not too far from $\mathbf{A}_{cc}$. Our approach provides no formal guarantee that the time-mean $\mathbf{A}$ is close to $\mathbf{A}_{cc}$. But, through the tuning of CIN_c, $\mathbf{A}_0$, and $\Delta\tau$, the time-mean $\mathbf{A}$ can be tuned to be close to the observed time mean.

Other cumulus parameterization schemes such as the Kuo scheme and the Betts–Miller scheme—by adjusting toward the onset criterion—also share the same non-catastrophe characteristics as the Arakawa–Schubert scheme and therefore suffer the same problems of incorrect phase and weak amplitude in the PDC. The prognostic closure approach (Randall and Pan 1993; Pan and Randall 1998) also has difficulty in simulating PDC [Fig. 7 of Lin et al. (2000)].

6. Test results

The GEOS-5 GCM, which is used for this study, has the finite-volume dynamical core of Lin (2004), the combined boundary layer and turbulence packages of Louis (1979) and Lock et al. (2000), the land surface model of Koster and Suarez (1996), the radiation package of Chou and Suarez (1994, 1999), RAS, and the prognostic cloud scheme and the rain reevaporation scheme of Bacmeister et al. (2006). The cumulus momentum transport scheme advects momentum using the cumulus mass flux calculated in RAS. The gravity wave parameterization is based on McFarlane (1987) and Garcia and Boville (1994). The SST and surface conditions were specified from observations. The horizontal resolution used is 2° × 2.5° (latitude × longitude). There are 72 vertical levels. In the model version used for this study, the thermal effects of subgrid-scale orographic variation are parameterized (Chao 2012) to prevent excessive precipitation over high mountains. Molod et al. (2012) documented the version of the GEOS-5 GCM and its performance just prior to Chao's (2012) work. For later comparison, the phase and amplitude of the PDC of the Tropical Rainfall Measurement Mission (TRMM) data are given in Fig. 5.

We have conducted three 10-yr experiments. The first one, E1, is the control run using RAS. The second, E2, uses C-CUPs to replace RAS over land only. The third, E3, uses C-CUPs globally. E3 generates somewhat worse

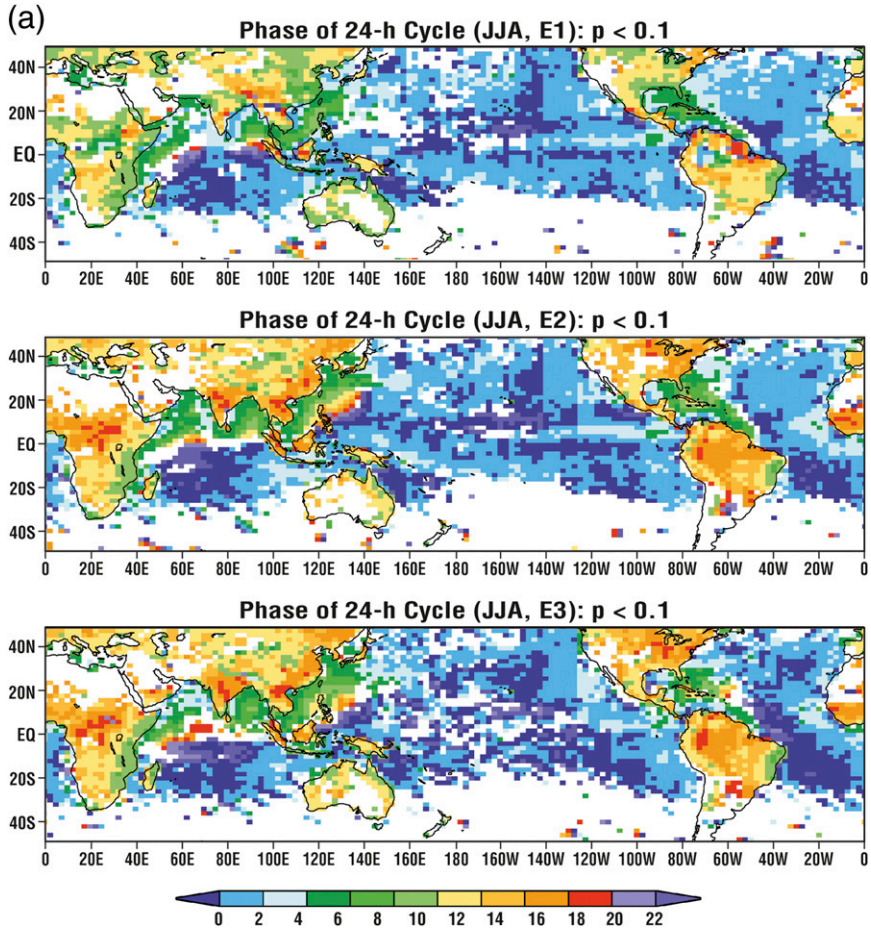

FIG. 6. (a) Phase and (b) amplitude (mm day^{-1}) of the precipitation diurnal cycle averaged over one JJA season for experiments (top) E1, (middle) E2, and (bottom) E3.

precipitation climatological results over the ocean than E2. Consequently, in the results discussed in this section we will mainly compare E2 with E1. This does not necessarily imply that the C-CUP concept does not work over the ocean. It only means that our particular C-CUP scheme is not well designed and/or well tuned for ocean grids. Since the PDC amplitude over the ocean is small, the problem with PDC when RAS is used is more prominent over land than over the ocean.

Figure 6 shows the comparison of the phase and amplitude of the PDC in the first June–August (JJA) season in E1 through E3. Data with a confidence level [as determined by the methodology described in the appendix of Lee et al. (2007a)] greater than 90% ($P = 0.1$) are presented. Figure 6 shows that over a large span of the land area in the tropics and subtropics, the peak of the PDC is between 1000 and 1400 LST in E1 and between 1600 and 2000 LST in E2. Also, over land the PDC amplitude is much larger in E2 than in E1 and is comparable to what is observed (Fig. 5). However, over steep and high mountains such as the Andes and the Himalayas, the PDC phase in E2 is still not correct. We will discuss this point in the next section.

The results in other years are very similar. In regions outside of high mountainous areas and outside of the ITCZ–monsoon and the midlatitude storm-track regions such as central Asia and southeastern Africa, there is no improvement in the PDC phase. This is because, in these regions, the large-scale precipitation is more dominant than the convective precipitation (a model defect that already existed prior to this work) and C-CUP has control only over the diurnal cycle of the latter.

Figure 7 shows the JJA 10-yr averaged precipitation in the three experiments and the comparison with the Global Precipitation Climatology Project (GPCP). It shows significant improvement in E2 over land, such as over southeastern portions of China and the United States, and the ITCZ regions over Africa and South America. Although there is some deterioration over the ocean, the standard deviation of the difference between

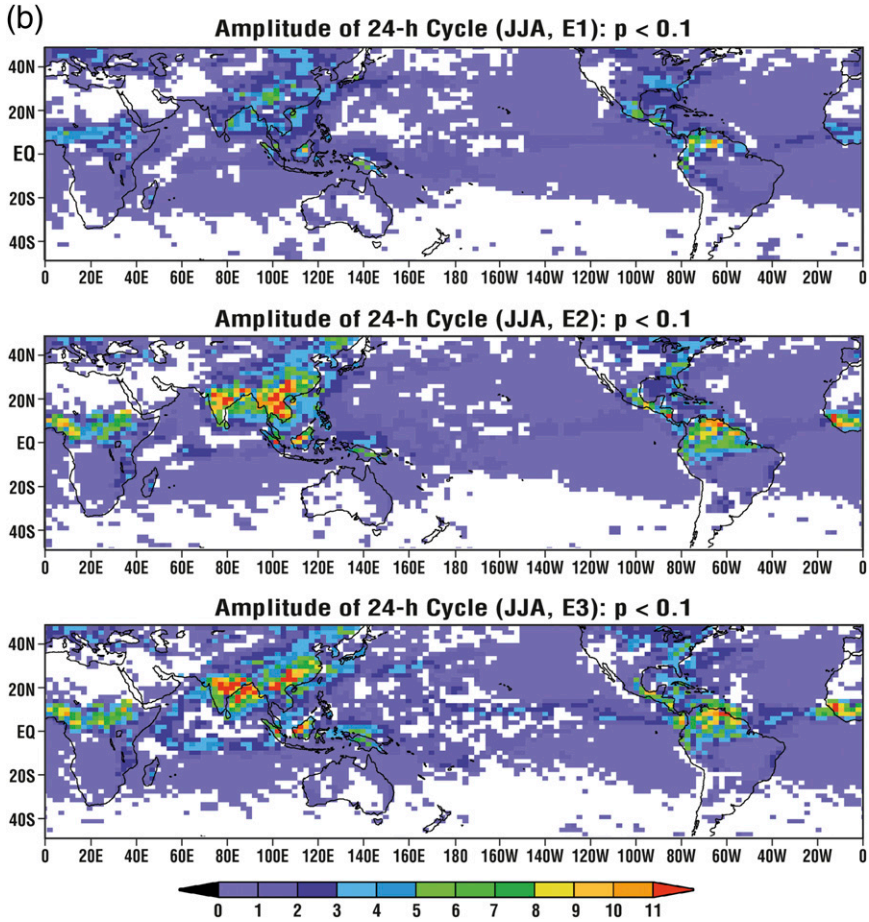

FIG. 6. (*Continued*)

the simulated results and GPCP observations (Fig. 7, bottom) barely worsens. E3 is clearly inferior to E2 with its larger departure from GPCP over the ocean. Table 1 shows the spatial- and time-mean root-mean-square error of various fields over ocean, land, and global domain [error is the difference between simulated monthly mean results and the observational monthly mean data, which are from GPCP for the precipitation data and from Modern-Era Retrospective Analysis for Research and Applications (MERRA) for the rest]. In general, Table 1 shows that over the ocean, E3 does not perform as well as E2. The reason for this deterioration in E3 is not yet understood.

Figure 8 shows the diurnal cycle of precipitation averaged over the JJA season for the 10-yr period in E1 (green curves), E2 (red curves), and E3 (blue curves) at four locations. The yellow curves depict the clear-sky downward solar radiative flux at the surface; their peaks indicate local noon. At all four locations the peak precipitation occurs around local noon in E1 and around 1600 LST in E2 and E3. The precipitation peaks in E2 and E3 are much sharper than that in E1. The larger daily averaged precipitation in E2 and E3 than in E1 over central and western Africa reflects changes in the ITCZ intensity and location.

In summary, the results show that C-CUPs is a significant improvement over RAS in terms of PDC simulation over relatively flat land. C-CUPs also reduces the systematic error in precipitation over land. The impact of C-CUPs on the other fields is mixed and modest.

7. Remarks and summary

The information about CIN and CAPE offered by Fig. 2 could also be obtained from observations, if the observations had a time interval of 1 h or less and enough density. Unfortunately, upper-air soundings are not available at such frequency and density. This demonstrates the value of CRMs.

In terms of performance a direct comparison of our C-CUPs with the wake and CIN–TKE approaches is difficult at this time, since the published works on these

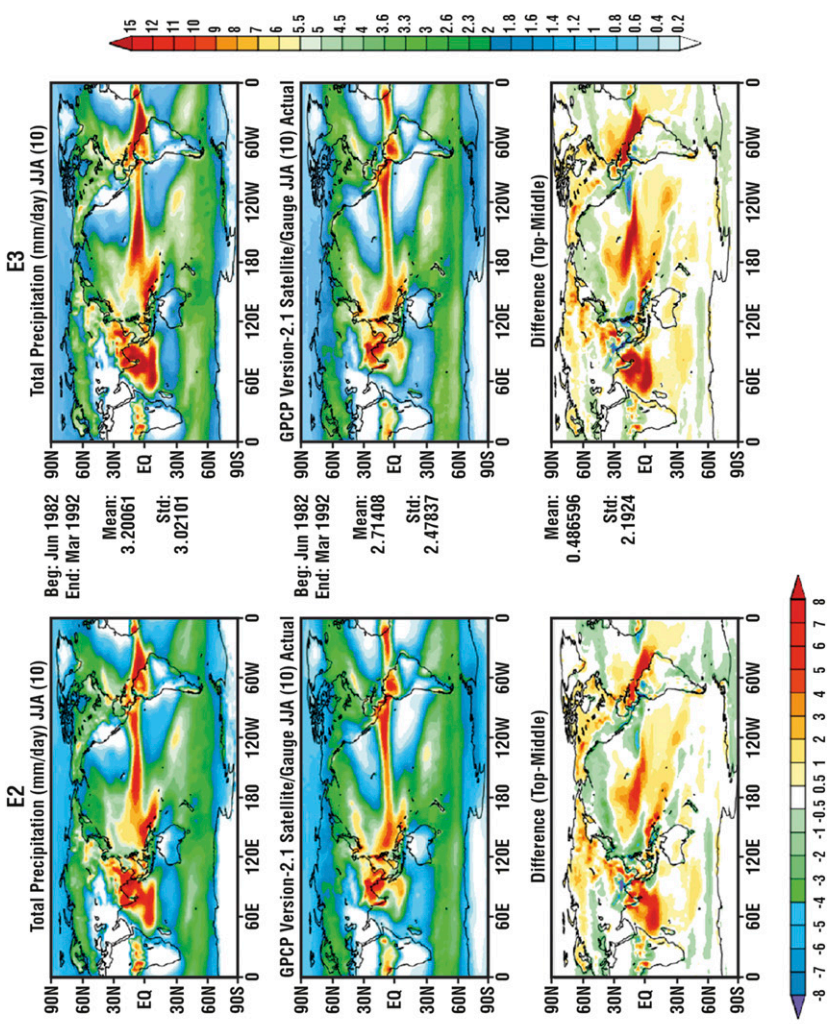

FIG. 7. Precipitation (mm day^{-1}) averaged over (top) 10-yr JJA season and (middle) the corresponding GPCP observation and (bottom) the difference between (top) and (middle) for experiments (left) E1, (middle) E2, and (right) E3.

TABLE 1. Spatial- and time-mean root-mean-square error for various fields [error being the difference between the monthly means of the simulated and the observed (GPCP for precipitation and MERRA for others) 10-yr data]. Eddy is the deviation from zonal mean. Values are given in the global (ocean only, land only) format.

	Control (E1)	C-CUPs over land (E2)	C-CUPs over globe (E3)
December–February (DJF)			
Precipitation (mm day^{-1})	2.298 (2.393, 2.104)	2.323 (2.572, 1.749)	2.459 (2.766, 1.724)
500-hPa height (m)	71.12 (65.21, 81.26)	72.42 (67.19, 81.52)	76.89 (72.56, 84.56)
500-hPa eddy height (m)	51.49 (49.99, 54.26)	51.65 (49.94, 54.78)	53.72 (52.09, 55.71)
500-hPa temperature (K)	2.939 (2.515, 3.533)	2.994 (2.673, 3.529)	3.082 (2.754, 3.628)
Sea level pressure (hPa)	6.600 (6.681, 6.443)	6.593 (6.784, 6.209)	6.936 (6.993, 6.827)
JJA			
Precipitation (mm day^{-1})	2.374 (2.437, 2.247)	2.464 (2.632, 2.106)	2.668 (2.909, 2.129)
500-hPa height (m)	65.76 (65.28, 66.67)	64.93 (65.06, 64.70)	64.384 (64.95, 63.28)
500-hPa eddy height (m)	46.81 (49.53, 41.09)	45.88 (48.22, 41.01)	45.375 (47.65, 40.65)
500-hPa temperature (K)	2.367 (2.247, 2.445)	2.334 (2.278, 2.437)	2.393 (2.392, 2.406)
Sea level pressure (hPa)	6.139 (6.203, 6.015)	6.301 (6.483, 5.938)	6.461 (6.537, 6.314)

approaches have thus far been only applied to single-column models, not GCMs. Moreover, the tuning work in C-CUPs has not been exhaustive and there is room for improvement simply through better tuning.

a. PDC over the ocean

Over the ocean the simulation of PDC is quite a different problem from that over land for two reasons. First, the PDC over the ocean is due to a combination of several different mechanisms. In relatively calm regions, a peak appears in the late afternoon corresponding to the SST diurnal cycle, which is under strong solar forcing in less cloudy conditions. In strongly convectively active regions, there is little PDC; the convection is interacting and phase locked with the westward-moving 2-day inertial–gravity waves (Chen and Houze 1997). The convection starts in late afternoon and peaks in the predawn hours and there is little convection the next day. There can also

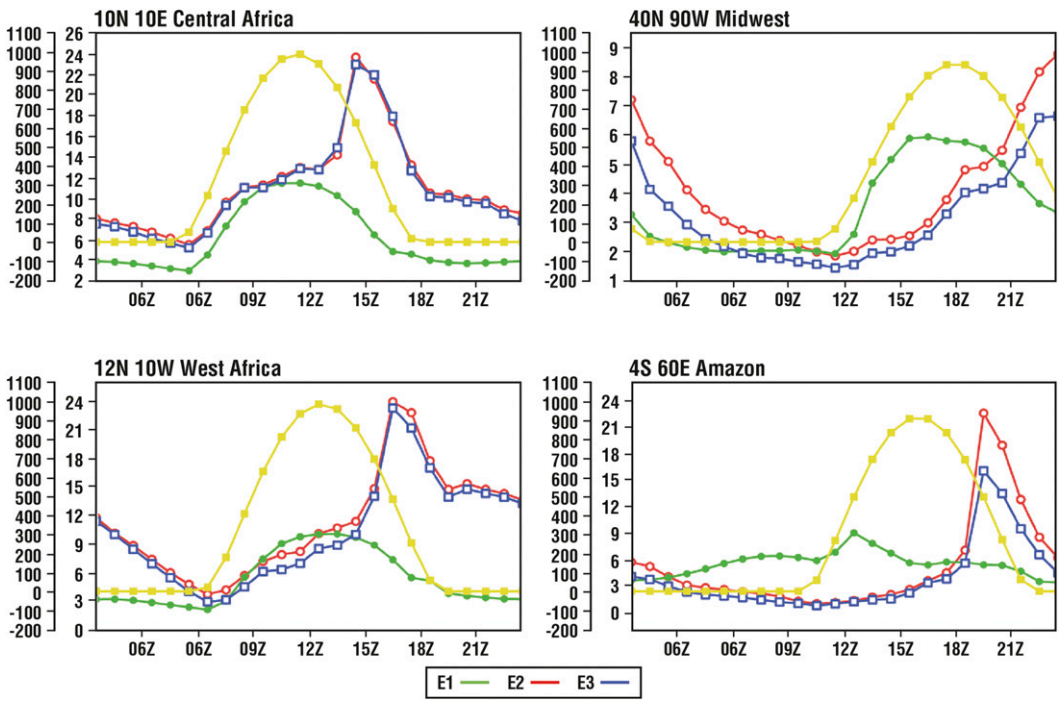

FIG. 8. 10-yr JJA-averaged precipitation diurnal cycle (right scale; mm day^{-1}) for E1 (green), E2 (red), and E3 (blue) for various locations. The yellow curves show the diurnal cycle of clear-sky downward solar radiation (left scale; W m^{-2}) at the surface; their peaks show the time of local noon. The labels for the *x* axis give the time (UTC).

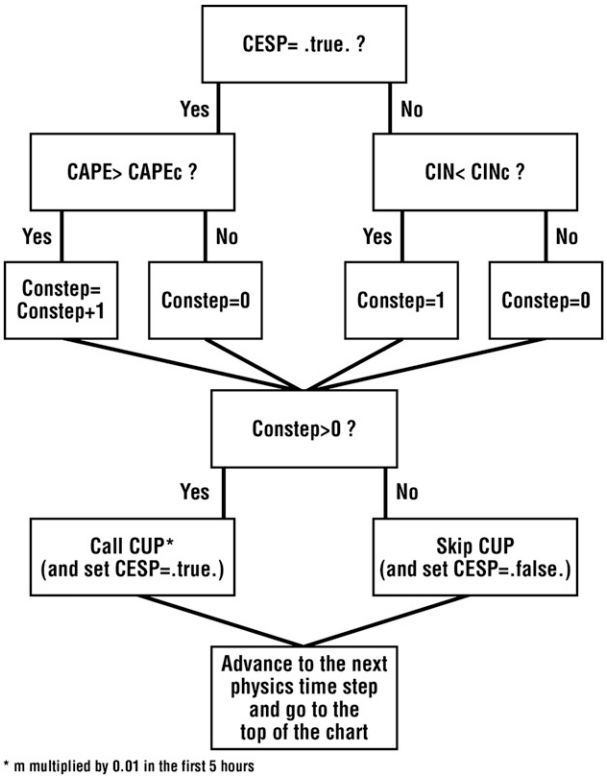

FIG. A1. Flowchart of the C-CUPs computational procedure.

be a diurnal peak—associated with shallow clouds—in the early morning hours (0000–0600 LST) reacting to the nighttime radiative cooling.

Second, the PDC over the ocean has a much lower amplitude than over land. This makes its GCM simulation more difficult than over land. Apparently, our solution, though helpful over land, is not sufficient to handle the PDC over the ocean. Additional adjustments in model physics, which are not yet understood, are needed. These will be left for future research.

b. PDC over mountainous regions

PDC over mountainous regions such as the Sierra Madre, the Andes, and the Himalayas is different from that over relatively flat land. Our results have failed in simulating PDC peaks that occur after 2200 LST over mountainous regions. Mountain slopes that are resolved by the model generate upslope boundary layer winds because of their thermal effects. Also, subgrid-scale mountains can generate subgrid-scale vertical circulation that transfers heat from the boundary layer to the layers high above. Chao (2012) has designed a subgrid-scale heated-slope-induced vertical circulation (SHVC) parameterization scheme, which has been used in all experiments in this work, to incorporate the thermal effects of the subgrid-scale topographic variation into a GCM in order to prevent excessive precipitation over steep and high mountains. With or without the SHVC parameterization, the boundary layer over the mountainous areas does not heat up during the day as much as over relatively flat land because of the heat removal (to a large extent) by thermally forced upslope winds in the boundary layer along the mountain slopes. Thus, the PDC over the mountainous regions is governed by a different mechanism from that over relatively flat land. The nature of this mechanism is being explored. As an aside, the general reduction of precipitation over land due to the use of C-CUPs has led to a slight precipitation deficit over high mountains, such as the Himalayas and the Andes, but this can be easily remedied by reducing the dosage of the SHVC parameterization.

c. Other possible future research directions

Our use of CAPE $<$ CAPE$_c$ as the convective termination criterion is only a modeling measure. The detailed process of convective termination is not well known and needs to be understood. Only after convective termination can CIN reassert its suppressing role. The eastward propagation of convection in the JJA season over the central United States starting from the eastern slopes of the Rockies (e.g., Tripoli and Cotton 1989a,b; Yang and Smith 2006) has not been successfully simulated in the GEOS-5 GCM. Its correct simulation is another interesting future direction. This failure may be linked to the simulation of PDC over high and steep mountains, where such propagation starts. Another reason for this failure could be the coarse resolution used. The minimal grid size for which our cumulus parameterization still works remains to be determined. Also, what further modification of our design of cumulus parameterization is needed for a grid size on the order of 5–25 km is another interesting future direction. Evaluation of C-CUPs' performance, when it is used both over both land and ocean, in simulating equatorial waves, MJO, tropical cyclones, easterly waves, monsoons, monsoon onset, etc. would also be good future directions. Finally, how C-CUPs impacts the weather forecast capability and the data assimilation products should also be studied.

To summarize, this study demonstrates that replacement of the noncatastrophe concept with the catastrophe concept in cumulus parameterization leads to improvement in the simulation of PDC over relatively flat land. The core of this replacement has two components: 1) recognition of the role of convective inhibition in the suppression of cumulus convection in a grid column and the irrelevance of convective inhibition once the onset commences and 2) cumulus convection adjusts the state of the grid column toward the convection termination criterion, which is different from the onset criterion.

Acknowledgments. Technical help from Larry Takacs and Max Suarez, both of NASA GSFC GMAO, in using the GEOS-5 GCM is gratefully acknowledged. Myong-In Lee generously provided Fig. 5 and the postprocessing computer program that produced Fig. 6. Suggestions from Michele Rienecker and Kay Cheney improved the manuscript writing. W. W. Grabowski and P. A. Dirmeyer and two anonymous reviewers provided helpful reviews of the manuscript. This work was supported by NASA's Modeling, Analysis, and Prediction program under WBS 802678.02.17.01.25. Computing resources supporting this work were provided by the NASA High-End Computing (HEC) Program through the NASA Center for Climate Simulation (NCCS) at Goddard Space Flight Center.

APPENDIX

Flowchart of the C-CUPs Computational Procedure

Figure A1 shows the computational procedure used in C-CUPs.

REFERENCES

Arakawa, A., 2004: The cumulus parameterization problem: Past, present, and future. *J. Climate,* **17,** 2493–2525.

——, and W. H. Schubert, 1974: The interaction of a cumulus ensemble with the large-scale environment. Part I. *J. Atmos. Sci.,* **31,** 674–701.

Bacmeister, J. T., M. J. Suarez, and F. R. Robertson, 2006: Rain reevaporation, boundary layer–convection interactions, and Pacific rainfall patterns in an AGCM. *J. Atmos. Sci.,* **63,** 3383–3403.

Bechtold, P., J. P. Charoureau, A. Beljaars, A. K. Betts, M. Köhler, M. Miller, and J.-L. Redelsperger, 2004: The simulation of the diurnal cycle of convective precipitation over land in a global model. *Quart. J. Roy. Meteor. Soc.,* **130,** 3110–3137.

Chaboureau, J.-P., F. Guichard, J.-L. Redelsperger, and J.-P. Lafore, 2004: The role of stability and moisture in the diurnal cycle of convection over land. *Quart. J. Roy. Meteor. Soc.,* **130,** 3105–3117, doi:10.1256/qj.03.132.

Chao, W. C., 1985: Stratospheric sudden warmings as catastrophes. *J. Atmos. Sci.,* **42,** 1631–1646.

——, 2008: Understanding atmospheric catastrophes. *Recent Progress in Atmospheric Sciences: Applications to the Asia–Pacific Region,* K.-N. Liou and M.-D. Chou, Eds., World Scientific, 89–103.

——, 2012: Correction of excessive precipitation over steep and high mountains in a GCM. *J. Atmos. Sci.,* **69,** 1547–1561.

Chen, S. S., and R. A. Houze, 1997: Diurnal variation and life-cycle of deep convective systems over the tropical Pacific warm pool. *Quart. J. Roy. Meteor. Soc.,* **123,** 357–388.

Chou, M.-D., and M. J. Suarez, 1994: An efficient thermal infrared radiation parameterization for use in general circulation models. Technical Report Series on Global Modeling and Data Assimilation, Vol. 3, NASA Tech. Memo. NASA/TM-104606, 102 pp. [Available online at http://gmao.gsfc.nasa.gov/pubs/tm/docs/Chou128.pdf.]

——, and ——, 1999: A solar radiation parameterization for atmospheric studies. Technical Report Series on Global Modeling and Data Assimilation, Vol. 15, NASA Tech. Memo. NASA/TM-1999-104606, 40 pp. [Available online at http://gmao.gsfc.nasa.gov/pubs/tm/docs/Chou136.pdf.]

Dai, A., F. Giorgi, and K. E. Trenberth, 1999: Observed and model-simulated diurnal cycles of precipitation over the contiguous United States. *J. Geophys. Res.,* **104** (D6), 6377–6402.

Dirmeyer, P. A., and Coauthors, 2012: Simulating the diurnal cycle of rainfall in global climate models: Resolution versus parameterization. *Climate Dyn.,* **39,** 399–418, doi:10.1007/s00382-011-1127-9.

Emanuel, K. A., 1991: A scheme for representing cumulus convection in large-scale models. *J. Atmos. Sci.,* **48,** 2313–2335.

Garcia, R. R., and B. A. Boville, 1994: Downward control of the mean meridional circulation and temperature distribution of the polar winter stratosphere. *J. Atmos. Sci.,* **51,** 2238–2245.

Grabowski, W. W., and Coauthors, 2006: Daytime convective development over land: A model intercomparison based on LBA observations. *Quart. J. Roy. Meteor. Soc.,* **132,** 317–344.

Grandpeix, J.-Y., and J.-P. Lafore, 2010: A density current parameterization coupled with Emanuel's convection scheme. Part I: The models. *J. Atmos. Sci.,* **67,** 881–897.

Guichard, F., and Coauthors, 2004: Modelling the diurnal cycle of deep precipitating convection over land with cloud-resolving models and single-column models. *Quart. J. Roy. Meteor. Soc.,* **130,** 3139–3172.

Hohenegger, C., and C. S. Bretherton, 2011: Simulating deep convection with a shallow convection scheme. *Atmos. Chem. Phys.,* **11,** 10 389–10 406.

Houze, R. A., 1977: Structure and dynamics of a tropical squall line system. *Mon. Wea. Rev.,* **105,** 1540–1567.

Jones, T. R., and D. A. Randall, 2011: Quantifying the limits of convective parameterizations. *J. Geophys. Res.,* **116,** D08210, doi:10.1029/2010JD014913.

Khairoutdinov, M. F., and D. A. Randall, 2006: High-resolution simulation of shallow-to-deep convection transition over land. *J. Atmos. Sci.,* **63,** 3421–3436.

——, C. A. DeMott, and D. A. Randall, 2008: Evaluation of the simulated interannual and subseasonal variability in an AMIP-style simulation using the CSU multiscale modeling framework. *J. Climate,* **21,** 413–431.

Koster, R. D., and M. J. Suarez, 1996: Energy and water balance calculations in the Mosaic LSM. Technical Report Series on Global Modeling and Data Assimilation, Vol. 9, NASA Tech Memo. 104606, 76 pp. [Available online at http://gmao.gsfc.nasa.gov/pubs/tm/docs/Koster130.pdf.]

Kuang, Z., and C. S. Bretherton, 2006: A mass-flux scheme view of a high-resolution simulation of a transition from shallow to deep cumulus convection. *J. Atmos. Sci.,* **63,** 1895–1909.

Lee, M.-I., and Coauthors, 2007a: Sensitivity to horizontal resolution in the AGCM simulations of warm season diurnal cycle of precipitation over the United States and northern Mexico. *J. Climate,* **20,** 1862–1881.

——, S. D. Schubert, M. J. Suarez, T. L. Bell, and K.-M. Kim, 2007b: The diurnal cycle of precipitation in the NASA Seasonal to Interannual Prediction Project atmospheric general circulation model. *J. Geophys. Res.,* **112,** D16111, doi:10.1029/2006JD008346.

Lin, S.-J., 2004: A "vertically Lagrangian" finite-volume dynamical core for global models. *Mon. Wea. Rev.,* **132,** 2293–2307.

Lin, X., D. A. Randall, and L. D. Fowler, 2000: Diurnal variability of the hydrologic cycle and radiative fluxes: Comparisons between observations and a GCM. *J. Climate,* **13,** 4159–4179.

Lock, A. P., A. R. Brown, M. R. Bush, G. M. Martin, and R. N. B. Smith, 2000: A new boundary layer mixing scheme. Part I: Scheme description and single-column model tests. *Mon. Wea. Rev.,* **128,** 1387–1399.

Lord, S. J., W. C. Chao, and A. Arakawa, 1982: Interaction of a cumulus cloud ensemble with the large-scale environment. Part IV: The discrete model. *J. Atmos. Sci.,* **39,** 104–113.

Louis, J. F., 1979: A parametric model of vertical eddy fluxes in the atmosphere. *Bound.-Layer Meteor.,* **17,** 187–202.

Mapes, B. E., 1997: Equilibrium vs. activation control of large-scale variations of tropical deep convection. *The Physics and Parameterization of Moist Atmospheric Convection,* R. K. Smith, Ed., NATO ASI Series C, Vol. 505, Kluwer Academic Publishers, 321–358.

——, and R. Neale, 2011: Parameterizing convective organization to escape the entrainment dilemma. *J. Adv. Model. Earth Syst.,* **3,** M06004, doi:10.1029/2011MS000042.

McFarlane, N. A., 1987: The effect of orographically excited gravity wave drag on the general circulation of the lower stratosphere and troposphere. *J. Atmos. Sci.,* **44,** 1775–1800.

Molod, A., L. Takacs, M. Suarez, J. Bacmeister, I.-S. Song, and A. Eichmann, 2012: The GEOS-5 atmospheric general circulation model: Mean climate and development from MERRA to Fortuna. Technical Report Series on Global Modeling and Data Assimilation, Vol. 28, NASA Tech. Memo. NASA/TM–2012-104606. [Available online at http://gmao.gsfc.nasa.gov/pubs/docs/Molod484.pdf.]

Moorthi, S., and M. J. Suarez, 1992: Relaxed Arakawa–Schubert: A parameterization of moist convection for general circulation models. *Mon. Wea. Rev.,* **120,** 978–1002.

Pan, D.-M., and D. A. Randall, 1998: A cumulus parameterization with a prognostic closure. *Quart. J. Roy. Meteor. Soc.,* **124,** 949–981.

Pritchard, M. S., and R. C. J. Somerville, 2009: Assessing the diurnal cycle of precipitation in a multi-scale climate model. *J. Adv. Model. Earth Syst.,* **1** (12), doi:10.3894/JAMES.2009.1.12.

Putman, W. M., and M. J. Suarez, 2011: Cloud-system resolving simulations with the NASA Goddard Earth Observing System global atmospheric model (GEOS-5). *Geophys. Res. Lett.,* **38,** L16809, doi:10.1029/2011GL048438.

Randall, D. A., and D.-M. Pan, 1993: Implementation of the Arakawa-Schubert cumulus parameterization with a prognostic closure. *The Representation of Cumulus Convection in Numerical Models, Meteor. Monogr.,* No. 46, Amer. Meteor. Soc., 137–144.

——, Harshvardhan, and D. A. Dazlich, 1991: Diurnal variability of the hydrological cycle in a general circulation model. *J. Atmos. Sci.,* **48,** 40–62.

Rio, C., F. Hourdin, J.-Y. Grandpeix, and J.-P. Lafore, 2009: Shifting the diurnal cycle of parameterized deep convection over land. *Geophys. Res. Lett.,* **36,** L07809, doi:10.1029/2008GL036779.

Satoh, M., T. Matsuno, H. Tomita, H. Miura, T. Nasuno, and S. Iga, 2008: Nonhydrostatic icosahedral atmospheric model (NICAM) for global cloud resolving simulations. *J. Comput. Phys.,* **227,** 3486–3514.

Schubert, W. H., 2000: A retrospective view of Arakawa's ideas on cumulus parameterization. *General Circulation Model Development,* D. A. Randall, Ed., Academic Press, 181–198.

Tao, W.-K., and Coauthors, 2009: A multiscale modeling system: Developments, applications, and critical issues. *Bull. Amer. Meteor. Soc.,* **90,** 519–534.

Tripoli, G. J., and W. R. Cotton, 1989a: Numerical study of an observed orogenic mesoscale convective system. Part I: Simulated genesis and comparison with observations. *Mon. Wea. Rev.,* **117,** 273–304.

——, and ——, 1989b: Numerical study of an observed orogenic mesoscale convective system. Part II: Analysis of governing dynamics. *Mon. Wea. Rev.,* **117,** 305–328.

Xu, K.-M., A. Arakawa, and S. K. Krueger, 1992: The macroscopic behavior of cumulus ensembles simulated by a cumulus ensemble model. *J. Atmos. Sci.,* **49,** 2402–2420.

Yang, S., and E. Smith, 2006: Mechanisms for diurnal variability of global tropical rainfall observed from TRMM. *J. Climate,* **19,** 5190–5226.